https://doi.org/10.1051/e3sconf/202124603003

Parametric Cost Optimization of Solar Systems with Seasonal Thermal Energy Storage for Buildings

Willy Villasmil*, *Marcel* Troxler, *Reto* Hendry, *Philipp* Schuetz, and *Jörg* Worlitschek

School of Engineering and Architecture, Lucerne University of Applied Sciences and Arts, 6048 Horw, Switzerland

Abstract. In combination with seasonal thermal energy storage (STES), solar energy offers a vast potential for decarbonizing the residential heat supply. In this work, a parametric optimization is conducted to assess the potential of reducing the costs of water-based STES through the use of alternative thermal insulation materials and the integration of an underground storage outside the building. The investigated configurations include: a hot-water tank, a solar collector installation, and a multifamily building with a solar fraction of 100%. The storage is either integrated inside the building or buried underground in its direct vicinity. A simulation-based analysis shows that if the tank is integrated inside an existing building (as part of a retrofitting action) – where costs are primarily driven by the loss of living space – vacuum-insulation panels can lead to significant savings in living space and a cost advantage compared to the use of conventional glass wool. Nevertheless, storage integration inside an existing building is a more expensive option compared to an external integration due to the high costs associated to the internal building modification and loss of living space. Despite the high excavation costs and increased heat losses, the concept of burying the storage underground is a promising option to allow the integration of large-volume seasonal storage systems in new and existing buildings.

1 Introduction

In combination with seasonal thermal energy storage (STES), solar heating systems offer a sustainable path for the decarbonization of the energy supply for space heating (SH) and domestic hot water (DHW) production in the residential sector. Space and water heating are responsible for round 80% of the energy needs of residential buildings in Europe [1] and 62% in the United States [2]. While solar technologies are becoming and more efficient and cost-effective, their inherent intermittent nature becomes a hurdle for their direct utilization. Through the application of STES the mismatch between the high solar gains in summer and the high heat demand in winter can be effectively balanced, overcoming thereby the above limitation.

Despite its technological maturity, water-based seasonal heat storage systems have been implemented only in handful of projects. Examples of such projects are the solar houses in Bern (CH) with storage volumes in the range 100 – 200 m^3 and very high solar fractions [3], [4]. The challenge of such projects is that the specific investment costs for storage facilities of this size are significantly higher than for storage facilities of 10 to 100 times higher capacity [5], [6]. In fact, the problem of reaching an increased market diffusion of STES is not attributed to a lack of knowledge of these technologies – which is considered to be high – but rather to their high cost [7].

Among various relevant design parameters, thermal insulation typically plays an important role in the cost optimization of STES systems [8]. The selection and specification of the insulation system (materials and thermal resistance) not only has an influence on investment costs, but it directly impacts the thermal efficiency of the storage system. Particularly in the case of water-based STES, where temperatures above 90 °C are common in order to maximize the storage capacity, minimizing the annual heat losses while ensuring the economic feasibility of the storage becomes of paramount importance. These conflicting requirements lead to an optimization problem in which the costs of the insulation and the storage container need to be balanced against the penalty costs associated to the annual heat losses and the space occupied by the storage system. The latter is particularly important when the storage is placed inside the building.

In this work, a parametric optimization is conducted to assess the potential of reducing the costs of water-based STES by using alternative thermal insulation materials and integrating an underground storage outside the building. The investigated configurations include the storage, a solar thermal collector system, and a low-energy multifamily building with a solar fraction of 100%.This contribution is organized as follows: In Section 2, the system and the scenarios considered for the optimization are described. In Section 3, the model platform and the models of the individual sub-systems and components are presented. Section 4 describes the methodology and the cost model, while Section 5 presents the results and discussion. In Section 6, conclusions of the obtained results are drawn.

*Corresponding author: willy.villasmil@hslu.ch

2 System description

The investigated configuration comprises three sub-systems: (i) a seasonal, hot-water thermal energy storage, (ii) a solar thermal collector system, and (iii) a low-energy multifamily building. The storage and solar collectors are dimensioned such that an annual solar fraction of 100% is achieved – i.e. the building's heat demand for space heating (SH) and domestic hot water (DHW) is covered solely by solar energy.

The tank-in-tank storage configuration contains four helical heat exchangers (HEX) for transferring the heat harvested by the solar collectors to the storage, three cylindrical vessels (VSL) for producing and storing DHW, and four inflow/outflow ports (POR) for supplying hot water to the SH system.

The glazed flat plate solar collectors represent the only heat source in the system. They are operated such that the temperature of the heat transfer fluid (HTF, a 40% glycol/ 60% water mixture) at the collector outlet does not exceed 110 °C at any point in time. Operating beyond this limit is considered unnecessary, as temperatures above 110 °C are only attainable in summer when the solar yield is anyhow high enough to fully charge the thermal energy storage.

The low-energy multifamily building is equipped with a radiant floor heating system connected to the storage via the inflow/outflow ports described above.

Two scenarios are considered in this work (see Fig. 1): (i) a storage tank integrated inside the building, and (ii) a storage tank buried underground in direct vicinity of the building. In both cases, the maximum storage temperature is limited to 90 °C. The scenarios differ mainly in the location of the storage and the thermal insulation used.

Scenario 1: Storage integrated inside the building

In this scenario, the storage consists of a cylindrical steel tank placed inside a shaft room in the middle of the building. The 15-m-high storage tank is placed in the building – extending from the basement to the topmost floor – to allow the thermal losses to cover a fraction of the space heating demand [9]. To avoid overheating of the building in summer, the tank is thermally insulated. In the forthcoming analysis, the steel tank is insulated using either: glass wool (GW), polyurethane foam (PUR) or vacuum insulated panels (VIP). A major drawback of this scenario is the loss of living space (and the associated cost penalties) that results from placing the storage inside an existing building. In this study, two cases are considered within this scenario:

- **Retrofit:** Integration of the STES system in an existing building. The loss in living space and the need for an internal reconstruction of the building translates into large penalty costs.
- **New building**: The STES system is integrated in a new building. In this case it is assumed that the floor area ratio is not affected by the storage and thus no penalty costs are incurred.

In this scenario, the building is also heated directly by means of the heat losses of the storage tank. Without specific counter-measures these heat losses cause a heating of the building in summer.

Scenario 2 - Storage buried underground

A vacuum-insulated steel tank is buried underground in direct vicinity of the building. The thermal insulation is realized by evacuating the volume between inner and outer shell of the tank. The evacuated envelop is filled with small particles with the aim of suppressing radiative heat transfer [10].

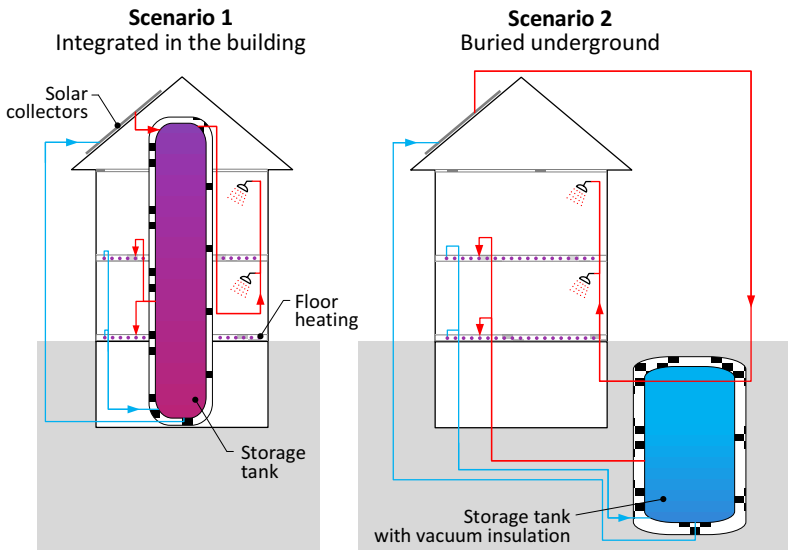

Figure 1. Considered scenarios. *Left*: storage integrated inside the building. *Right*: vacuum-insulated storage buried underground in direct vicinity of the building. The only external heat source is the solar collectors.

3 Numerical models

The performance of the solar heating system is investigated using an in-house finite-volume code written in C++. The dynamic system model consists of three coupled modules: (i) a stratified thermal energy storage model, (ii) a multi-family building model, and (iii) a solar collector model. The models use the following parameters as inputs: geometry characteristics, thermo-physical properties, performance characteristics of the solar collectors, weather data, DHW consumption profiles and number of occupants of the building. The main outputs of the model include the temperature distribution of the storage, the DHW and room temperatures and the various energy flows in and out of each of the system components.

3.1 Thermal energy storage model

The core of the 1D storage model consists of eight coupled energy conservation equations. The main equation describes the axial temperature distribution in the hot-water storage, while the other seven equations describe the internal sub-components – four heat exchangers (HEX) and three vessels (VSL). Source terms interlink HEX and VSL equations with the storage equation. The following energy conservation equation describes the temperature distribution in the storage:

$$\begin{aligned} m_{\mathrm{w}} c_{p,\mathrm{w}} \frac{\partial T_{\mathrm{tes}}}{\partial t} = \lambda_{\mathrm{w}} \frac{\partial^2 T_{\mathrm{tes}}}{\partial z^2} V_{\mathrm{tes}} - m_{\mathrm{w}} c_{p,\mathrm{w}} u \frac{\partial T_{\mathrm{tes}}}{\partial z} \\ + \sum_i U_{\mathrm{hex}}\, A_{\mathrm{hex}} (T_{\mathrm{tes}} - T_{\mathrm{hex}\text{-}i}) \\ + \sum_j U_{\mathrm{vsl}}\, A_{\mathrm{vsl}} \left(T_{\mathrm{tes}} - T_{\mathrm{vsl}\text{-}j}\right) \\ + \sum_k \dot{m}_k c_{p,\mathrm{w}} \left(T_{\mathrm{tes}} - T_{\mathrm{por}\text{-}k}\right) \\ - \dot{Q}_{\mathrm{tes,loss}} \end{aligned} \tag{1}$$

Where m_{w} is the mass of water, c_p the specific heat capacity, λ the thermal conductivity, T the fluid temperature, z the axial coordinate (starting at the bottom of the storage), u the axial fluid velocity inside the storage, U the overall heat transfer coefficient, A the heat transfer area, V_{tes} the storage volume, $\dot{m}_k$ the mass flow rate entering the storage through port k. The term $\dot{Q}_{\mathrm{tes,loss}}$ represents the heat losses from the storage to the surroundings. The index *w* refers to water, *por* to port, and *tes* to thermal energy storage. Further assumptions are made: (i) radial temperature gradients are neglected, (ii) no phase change occurs, (iii) all flows are fully developed. The various source terms in Eq. 1 represent:

- Energy exchange between the HTF in the HEXs and the water in the storage tank
- Energy exchange between the DHW in the VSLs and the water in the storage tank
- Energy exchange by means of extraction/insertion of water from/to the storage via the PORs
- Energy losses over the tank's outer surfaces

A node-mixing model is applied to determine the effects of buoyancy-induced mixing within the storage. Increases in fluid density cause cooler layers to sink and warmer layers to rise. The node-mixing model considers a point in time when a warmer layer $i+1$, positioned below a cooler layer i, completely mixes reaching a uniform temperature. This is expressed by:

$$T_i^{\mathrm{new}} = T_{i+1}^{\mathrm{new}} = \frac{m_i c_{p,i} T_i + m_{i+1} c_{p,i+1} T_{i+1}}{m_i c_{p,i} + m_{i+1} c_{p,i+1}} \tag{2}$$

If the temperature difference between two adjacent layers ($T_i - T_{i+1}$) is found to be less than 0.001 K, these layers are taken as equal and not mixed.

3.2 Solar collector model

The heat generated by a solar thermal panel is calculated via:

$$\begin{aligned} \dot{Q}_{\mathrm{col}} = \eta_0\, I A_{\mathrm{col}} - C_1 (\bar{T}_{\mathrm{col}} - T_{\mathrm{amb}}) A_{\mathrm{col}} \\ - C_2 (\bar{T}_{\mathrm{col}} - T_{\mathrm{amb}})^2 A_{\mathrm{col}} \end{aligned} \tag{3}$$

Where η_0 is the zero-loss collector efficiency constant, I the global solar irradiation at the considered location with the given panel orientation and inclination, $\bar{T}_{\mathrm{col}}$ the mean collector temperature, T_{amb} the ambient temperature, and A_{col} the collector aperture area. The parameters C_1 and C_2 are determined according to the European Standard EN 12975.

3.3 Building model

The dynamics of the building are modelled by an energy balance equation of the building in analogy to the work of [11], [12]. The state of the building is described by an average room temperature T_{room}. The building dynamics is modelled by treating the building as a single node with a lumped capacity C under the heat flux $\dot{Q}_{\mathrm{loss}}$ from losses through the walls, the solar heat flow $\dot{Q}_{\mathrm{solar}}$ through the windows into the building, the heat flow $\dot{Q}_{\mathrm{sh}}$ from the floor heating system and internal loads $\dot{Q}_{\mathrm{int}}$ from inhabitants and appliances, and the heat flow $\dot{Q}_{\mathrm{tes,loss}}$ from the thermal losses of the storage tank. Accordingly, the change of the room temperature is modelled as follows:

$$C \frac{\partial T_{\mathrm{room}}}{\partial t} = \dot{Q}_{\mathrm{loss}} + \dot{Q}_{\mathrm{solar}} + \dot{Q}_{\mathrm{sh}} + \dot{Q}_{\mathrm{int}} + \dot{Q}_{\mathrm{tes,loss}} \tag{4}$$

Thermal losses are modelled by a simplified heat transfer equation between room and environment as:

$$\dot{Q}_{\mathrm{loss}} = -H (T_{\mathrm{room}} - T_{\mathrm{amb}}) \tag{5}$$

with the ambient temperature T_{amb} and a lumped heat conductivity coefficient H. The solar contribution is modelled as follows:

$$\dot{Q}_{\mathrm{solar}} = g I_{\mathrm{win}} \tag{6}$$

with the solar contribution factor g of the windows and the solar radiation I_{win} falling on the windows of the building. The solar radiation considers the orientation of the building, the orientation and position of the windows as well as the position of the sun. The heat flux from the space-heating system is modelled by the radiator equation as follows:

$$\dot{Q}_{\mathrm{sh}} = \dot{Q}_{\mathrm{sh,design}} \left(\frac{\frac{T_{\mathrm{sh,in}} + T_{\mathrm{sh,out}}}{2} - T_{\mathrm{room}}}{\Delta T_{\mathrm{design}}} \right)^{n_r} \tag{7}$$

with $T_{\mathrm{sh,in}}$, $T_{\mathrm{sh,out}}$ the inlet and outlet temperature of the emitter system, $\dot{Q}_{\mathrm{sh,design}}$ the design power of the heating system at $\Delta T_{\mathrm{design}}$ temperature difference, and the radiator exponent $n_r = 1.1$ suitable for modelling floor heating systems.

4 Methodology

Yearly simulations were performed to determine the minimum storage volume required to achieve an annual solar fraction of 100%. The start of the simulated period was April 1st and a uniform storage temperature of 40 °C was taken as initial condition. For a given system configuration, the minimum storage volume required was found iteratively through variation of the storage diameter until the minimum temperature of the DHW produced throughout the year after the charging phase was equal to 60 °C. This was deemed as the minimum temperature required to satisfy hygienic standards for DHW production. At this condition, SH and DHW requirements are fulfilled with the smallest storage volume. The height of the storage tank was kept constant at 15 m for all configurations of scenario 1.

The key parameters used in the simulations have been summarized in Table 1. The reference multi-family house has a heated floor area of 924 m^2 distributed over four floors and a full-height basement. Bern (CH) was taken as the building reference location. A single thermal zone was used to represent the entire building. The house is heated to a set temperature of 20 ± 0.5 °C during the heating period. The DHW draw-off profiles were generated using the DHWcalc program (version 2.02b). The annual DHW-profile was scaled such that the average daily water consumption per occupant was 50 liters at 60 °C. The cold-water temperature of the household water supply system was taken constant at 10 °C throughout the year. The climate data used in the simulations consists of hourly mean values obtained with the Meteonorm database (version 7.1). The HTF of the solar collector loop was deemed a mixture of 60 vol% water and 40 vol% Glythermin P44 at 70 °C.

4.1 Target function

The cost of the system is used as the target function for the parametric-based optimization. Here, the target function is described by the Levelized Cost of Energy Storage at a solar fraction of 100% ($LCOES_{100}$):

$$\mathrm{LCOES}_{100} = \frac{C_{AF}}{E} = \frac{\mathrm{CAPEX} \cdot \mathrm{ANF} + \mathrm{OPEX}}{E} \qquad (8)$$

$LCOES_{100}$ describes the total cost per kWh of energy output, whereas C_{AF} is the annual full cost and E the annual useful energy output of the storage. The annuity factor (ANF) is given by:

$$\mathrm{ANF} = [(1+i)^n \cdot i]/[(1+i)^n - 1] \qquad (9)$$

where i is the interest rate and n is the payback period. Note that $LCOES_{100}$ is calculated based on the actual energy output of the storage and not the nominal storage capacity. Given the solar fraction of 100%, the energy output E equals the total annual heat demand. Capital expenditure (CAPEX) is calculated as the sum of costs of the building internal reconstruction (C_{const}, which only applies when the storage is incorporated inside an existing building), components (C_{com}), installation (C_{inst}), and loss of living space ($C_{\mathrm{imo,loss}}$):

$$\mathrm{CAPEX} = C_{\mathrm{const}} + C_{\mathrm{com}} + C_{\mathrm{inst}} + C_{\mathrm{imo,loss}} \qquad (10)$$

The cost of system components (C_{com}) are those of the solar collectors and the storage tank (including internal components such as heat exchangers). The costs for installation comprise the installation of the storage (in the building or underground) and the solar collector system. The component costs are given by the sum of the costs of the tank itself (C_{tank}), vessels (C_{VSL}), heat exchangers (C_{HEX}), thermal insulation (C_{ins}), and solar collectors (C_{sol}):

$$C_{\mathrm{com}} = C_{\mathrm{tank}} + C_{\mathrm{VSL}} + C_{\mathrm{HEX}} + C_{\mathrm{ins}} + C_{\mathrm{sol}} \qquad (11)$$

where the installation cost C_{inst} is split in two terms: the cost for installing the solar collectors ($C_{\mathrm{inst,sol}}$) and that for installing the storage itself ($C_{\mathrm{inst,TES}}$):

$$C_{\mathrm{inst}} = C_{\mathrm{inst,sol}} + C_{\mathrm{inst,TES}} \qquad (12)$$

Operational expenditures (OPEX) are calculated based on the capital expenditures of components and their installation using the operational factor β:

$$\mathrm{OPEX} = \beta(C_{\mathrm{com}} + C_{\mathrm{inst}}) \qquad (13)$$

The cost terms related to reconstruction work depend on the scenario under consideration:

- C_{const} (scenario 1, in the building): costs are calculated as a function of the number of floors

Table 1. Main parameters and characteristics of the building, the solar collector system, and the storage.

Building	
Heated floor area; number of occupants	924 m^2; 20
Window area and distribution	80 m^2 (55% south, 25% north, 10% east, 10% west)
Location and climate	
Location and altitude	Bern, Switzerland (46.93°N, 7.42°E), 565 m
Annual horizontal solar radiation	4.1 GJ/m^2
Solar thermal system	
Solar collector area	187 m^2 (orientation: facing south)
Collector parameters	$\eta_0 = 0.851$, $C_1 = 3.749$ W m^{-2} K^{-1}, $C_2 = 0.015$ W m^{-2} K^{-2}
Thermal energy storage	
Maximum storage temperature	90 °C
Storage height	15 m

(N_{floors}), the storage cross-sectional area (A_{TES}), and the reconstruction costs (c_{rec}):

$$C_{const,s1} = N_{floors} \cdot A_{TES} \cdot c_{rec} \quad (14)$$

where N_{floors} = 4 as the area lost in the basement is not accounted for.

- C_{const} (scenario 2, buried underground): in this case excavation costs are calculated as a function of the total storage volume (V_{TES}):

$$C_{const,s2} = V_{TES} \cdot c_{exc} \quad (15)$$

The volume specific are considered to increase linearly with the storage height of the storage.

Table 2 provides an overview of the values used for cost calculations. Values are based on commercial quotes and literature review. Estimates correspond to price levels in Switzerland.

5 Results and discussion

5.1 Scenario 1: storage in the building

The potential of reducing $LCOES_{100}$ with alternative thermal insulation materials is investigated – baseline is conventional glass wool (GW). In scenario 1, thermal insulation serves primarily the function of avoiding overheating of the building in summer. Figure 2 shows the maximum room temperature attained during summer as a function of the *R*-value of the thermal insulation. As a reference, the right axis shows the thickness of GW required to achieve a given *R*-value. At an insulation thickness of 80 cm, the required storage volume would be 157 m^3 and the maximum room temperature during summer would be essentially the same as if the storage would be placed outside the building (24 °C). Reducing the insulation thickness to 50 cm is expected to result in a temperature rise of less than 1 °C. Reducing the thickness further may lead to a significant temperature increase: at a thickness of 15 cm the required storage volume would be 207 m^3 and the room temperature could exceed the 30 °C limit. The required insulation thickness is thus dependent on the comfort penalties deemed acceptable and the additional costs that may result from the need for active cooling during summer.

In terms of the potential for cost reduction, Fig. 4 shows the $LCOES_{100}$ for the two cases of scenario 1 (retrofit and new building) along with the living space occupied by the storage as a function of the *R*-value. Results are shown for all thermal insulation materials investigated, namely GW (top), VIP (middle) and PUR (bottom). For a given temperature difference, heat losses from the storage are solely a function of the *R*-value. Hence, the minimum storage volume required to achieve a solar fraction of 100% is the same for a given *R*-value regardless of the thermal insulation material. However, due to the difference in thermal conductivity of the various insulation materials, the *total* volume occupied by the storage (i.e. storage volume plus insulation) changes with the material. Due to the low thermal conductivity of VIP, for example, storages equipped with VIP lead to the least loss of living space. At an *R*-value of 10 m^{2}K/W, using VIP instead of GW allows saving about 20 m^2 of living space.

The trends of the $LCOES_{100}$ curves are similar for all investigated thermal insulation materials. For the cases in which the storage is integrated in a new building, variation of the insulation thickness seems to have virtually no effect on the $LCOES_{100}$. This is presumably because cost savings associated to a smaller storage (as a result of reduced heat losses) are compensated by the additional costs associated to the thermal insulation itself. In the retrofit case, there seems to be an economic

Table 2. Main parameter used in the cost model. Values are based on commercial quotes and literature review.

C_{VSL}	18 EUR/l
C_{HEX}	$138 \cdot A_{HEX} + 129$ EUR
$C_{imo,loss}$	5'500 EUR/m^2
C_{ins}	GW: 100 EUR/m^3 PUR: 330 EUR/m^3 VIP: 3'700 EUR/m^3
$C_{inst,TES}$	$57 \cdot V_{tank} + 8300$ EUR
$C_{inst,ins}$	92 EUR/m^2
$C_{inst,sol}$	$239 \cdot A_{sol} + 8300$ EUR
C_{sol}	$280 \cdot A_{sol} + 180$ EUR
C_{tank}	Scenario 1: $430 \cdot V_{TES} + 1750$ EUR Scenario 2: $6350 \cdot V_{TES}^{0.504}$ EUR
c_{exc}	$55 \cdot H_{tank} + 92$ EUR/m^3
c_{rec}	2000 EUR/m^2
i	1%
n	20 years
β	Scenario 1: 0.005 (0.5%) Scenario 2: 0.02 (2.0%)

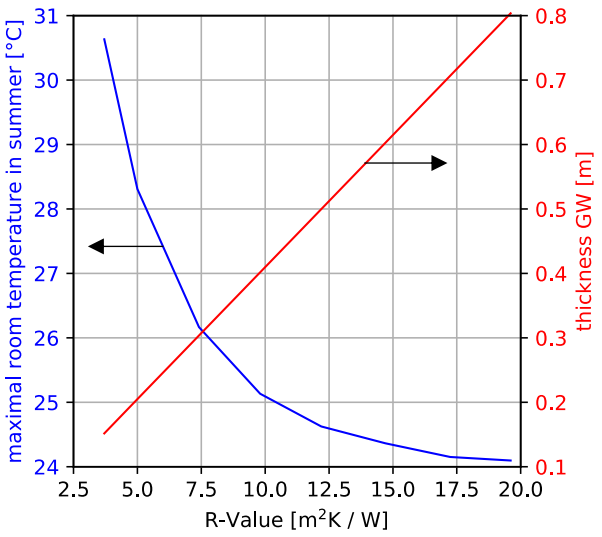

Figure 2. Maximal room temperature attained in summer as a function of the *R*-value of the thermal insulation. The right axis shows the thickness of GW required to achieve the corresponding *R*-value.

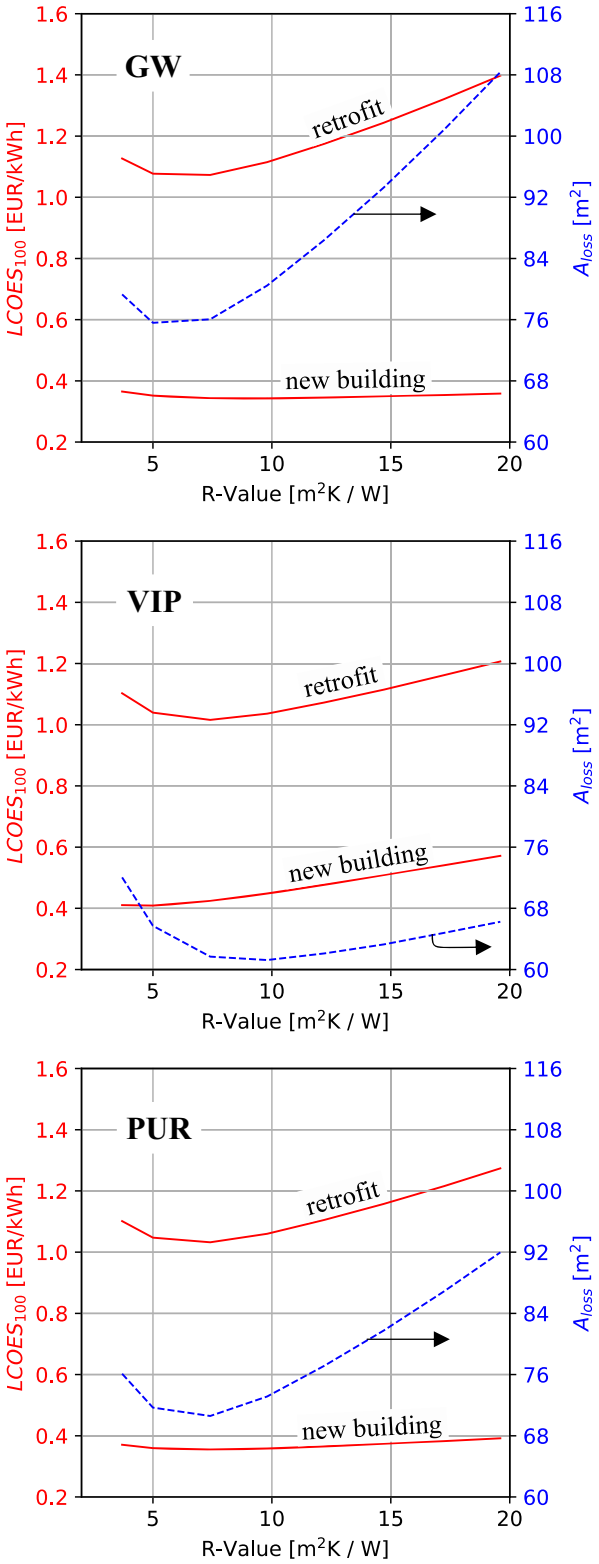

Figure 4. LCOES$_{100}$ for all three cases of scenario 1 (storage integrated in the building) as a function of the *R*-value of the thermal insulation. The right axis shows the extent of living space lost as a result of placing the storage tank inside the building. Thermal insulation applied to the storage: *top*: glass wool (GW); *middle*: VIP; *bottom*: PUR.

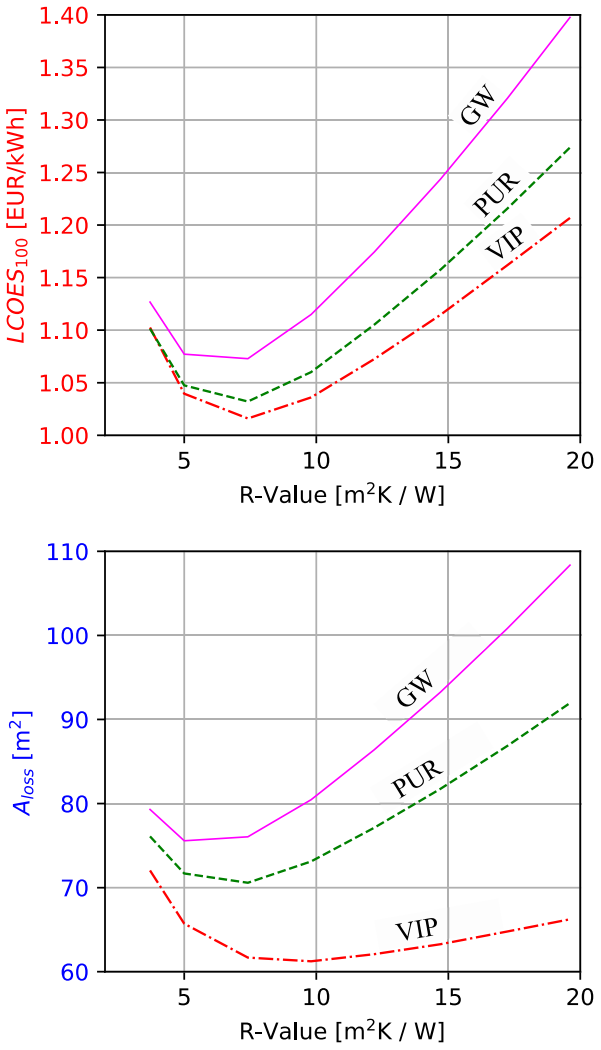

Figure 3. LCOES$_{100}$ and loss of living space (A_{loss}) as a function of *R*-value for each of the investigated thermal insulation materials. Scenario 1 (storage in building), retrofit case. Considered insulation materials: glass wool (GW), polyurethan foam (PUR) and vacuum-insulated panels (VIP).

optimum for the insulation thickness. A thinner insulation layer leads to the need for a larger storage (to compensate for increased heat losses), leading to a higher LCOES$_{100}$. With increasing insulation thickness the required storage volume is reduced and with it the LCOES$_{100}$ – up to an optimum at which LCOES$_{100}$ reaches its minimum. A further increase of the *R*-value would have only a marginal effect on the storage volume, which no longer outweighs the cost associated to the additional thermal insulation material. In the case of new buildings, storage tanks with a GW insulation of 40 cm exhibit the lowest LCOES$_{100}$ at 0.31 EUR/kWh.

In terms of the retrofit case, Fig. 3 shows LCOES$_{100}$ and the loss of living space for the three investigated thermal insulation materials as a function of the *R*-value. As a result of the high penalty costs associated to the loss of living space and the reconstruction costs of the building, the lowest LCOES$_{100}$ is reached with VIP in the retrofit case. The simulation results indicate that using a 9 cm layer of VIP would lead to a LCOES$_{100}$ of

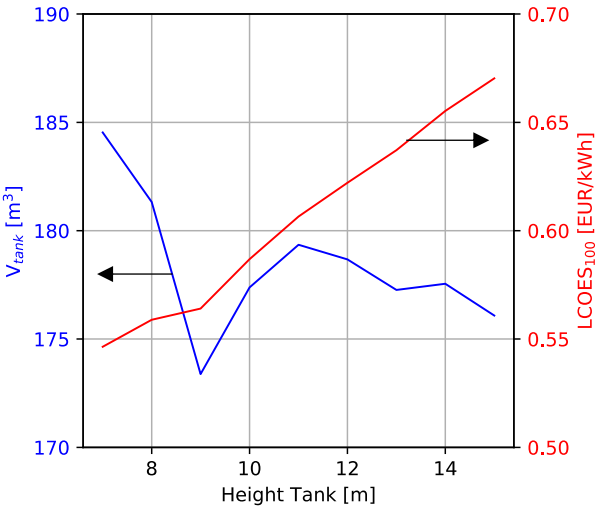

Figure 5. $LCOES_{100}$ and minimum required tank volume for scenario 2 (tank buried in the ground).

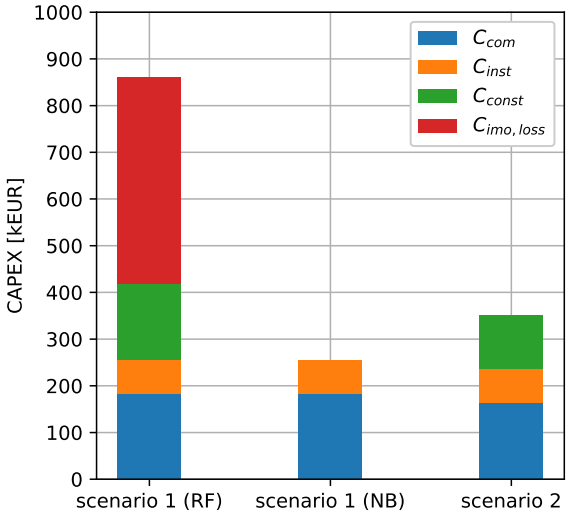

Figure 6. Breakdown of CAPEX. Scenario 1 includes the cases retrofit (RT) and new building (NB).

1.0 EUR/kWh and would allow saving about 14 m^2 of living space as compared to GW. As compared to VIP, PUR foams can offer a more reliable solution because of the uncertainties associated to the irreversible performance degradation of VIP. The use of PUR would lead to a $LCOES_{100}$ similar to that of VIP and could allow a small cost reduction of about 4% as compared to the use of GW.

In general, it is unlikely that the small cost benefit offered by VIP and PUR – as compared to glass wool – can justify the additional complexities and uncertainties associated to these alternative thermal insulation materials. Although PUR can offer a reliable solution (in terms of its long-term thermal stability), its main disadvantage is associated to the challenge of ensuring a proper installation (e.g. establishing a good contact between the insulation and the tank wall) to avoid thermal bridges. This may require the use of curved foams tailored to the tank geometry, which in turn are likely to increase material and installation costs.

5.2 Scenario 2: storage underground

The $LCOES_{100}$ of scenario 2, in which the storage is buried underground in direct vicinity of the building, is shown in Fig. 5. In Fig. 5, the blue curve (left axis) shows the minimum required storage volume, while the red curve (right axis) shows the calculated $LCOES_{100}$, both as a function of the tank height. Given that the heat losses in this case do not contribute to heating the building, the amount of energy to be provided to cover the SH demand is constant regardless of the tank configuration. The observed fluctuations in the storage volume are presumably the result of the different surface-to-volume ratios and the different dynamics within the storage due to the different heights (varying arrangement of the HEX and VES). By increasing the tank height from 7 to 15 m, the $LCOES_{100}$ is increased by approximately 20%. The reason for this significant increase is associated to the increased excavation costs that results when a deeper excavation is required.

5.3 Comparison of both scenarios

Table 3 shows a comparison of $LCOES_{100}$ and the various cost components for both scenarios. Scenario 1 includes the cases retrofit and new building. Given the solar fraction of 100% used as design requirement, the energy output of the storage (E) equals the building annual energy demand. For the simulated system, E was round 44'000 kWh – out of it, the DHW requirement accounted for 48%.

As compared to the $LCOES_{100}$ attained in the retrofit case of scenario 1 (1.1 EUR/kWh), this work indicates that the option of a vacuum-insulated storage buried underground may halve the $LCOES_{100}$ (0.55 EUR/kWh) by avoiding the high penalty costs associated to the loss of living space and the internal reconstruction of the building. In the case of a new building, both storage scenarios lead to $LCOES_{100}$ roughly in the range 0.4-0.6 EUR/kWh. Note that in calculating $LCOES_{100}$,

Table 3. $LCOES_{100}$, C_{AF}, OPEX and CAPEX obtained for the two scenarios investigated in this work.

	$LCOES_{100}$ [EUR/kWh]	C_{AF} [EUR/a]	OPEX [EUR/a]	CAPEX [kEUR]	OPEX/C_{AF} [%]
Scenario 1 (retrofit)	1.10	49'000	1'300	865'000	3
Scenario 1 (new building)	0.37	16'000	1'300	260'000	8
Scenario 2	0.55	24'000	4'800	350'000	20

OPEX has been assumed to be 4 times that of scenario 1 due to the lower TRL and increased maintenance required by the vacuum insulated storage. A 50% reduction in OPEX of scenario 2 – which is expected to happen as the technology continues to mature – would allow reducing $LCOES_{100}$ well below 0.5 EUR/kWh, making it more competitive. Although the storage integrated in the building offers the most cost-effective solution, this comes at the expense of additional heating during the summer season as a result of the unavoidable heat losses from the storage to its surroundings.

Figure 6 shows a breakdown of the total investment costs (including costs associated to loss of living space) for both scenarios. The costs of components and their installation is virtually the same for all cases, given that the solar collector system is the same and cost of the storage (incl. installation) only changes marginally between scenario 1 (130 kEUR) and scenario 2 (110 kEUR). Thus, the cost differences among the different cases are essentially driven by the loss of living space and the excavation costs.

6 Conclusions

In this work, a parametric-based optimization was conducted to assess the potential of reducing the costs of water-based seasonal thermal energy storage for low-energy multifamily houses. Two scenarios have been assessed: (i) storage integrated inside the building, and (ii) storage vessel buried underground in direct vicinity of the building. The investigated configurations included: (1) a hot-water storage tank, (2) a solar thermal collector installation, and (3) a multifamily building with a solar fraction of 100%.

The analysis included variation of the thermal insulation material, namely between glass wool (GW), polyurethane foam (PUR), and vacuum insulation panels (VIP). The use of vacuum-insulated storage vessels (a double-wall tank with an evacuated envelope) was evaluated as an alternative to allow integrating the storage underground and avoid thereby the loss of living space inside the building.

In the retrofit scenario, vacuum-insulation panels (VIP) – as an alternative to conventional glass wool – can lead to 20% savings in living space and a cost advantage of about 5%. In general, the small cost benefit offered by VIP and PUR – as compared to glass wool – is unlikely to justify the additional complexity and uncertainty associated to these alternative thermal insulation materials. At an $LCOES_{100}$ of round 1.0 EUR/kWh, the integration of the storage inside an existing building is the most expensive option due to the high costs associated to the internal modification of the building and the loss of living space. The $LCOES_{100}$ can be reduced by 50% if the storage is integrated inside a new building – mainly because of the high building reconstruction costs that are avoided.

As compared to the $LCOES_{100}$ attained in the retrofit case, the outcome of this work indicates that the option of burying a vacuum-insulated tank underground may halve the $LCOES_{100}$. Thus, commercially-available vacuum-insulated storages seem to be a promising solution for retrofit applications, as they offer the possibility of avoiding the high penalty costs associated to the loss of living space and the internal reconstruction of the building that is required when placing a large-volume tank inside an existing building. Moreover, a storage buried underground avoid the additional heating of the building during the summer season that results from the unavoidable heat losses from the storage to its surroundings.

The authors gratefully acknowledge the Swiss Federal Office of Energy for financial contributions to this work under the project OPTSAIS (project ID SI/501565-01). This research is part of the activities of the Swiss Competence Center for Energy Research on Heat and Electricity Storage (SCCER HaE), which is financially supported by the Swiss Innovation Agency – Innosuisse. The authors would like to thank the European commission for funding of the H2020-project "Heat4Cool" (project ID 723925). The work has also been supported by the Swiss State Secretariat for Education, Research and Innovation (SERI) under Contract No. 16.0082.

References

[1] Eurostat, "Energy consumption in households (EU-28, 2016 data)," 2018. https://ec.europa.eu/eurostat/statistics-explained/index.php/Energy_consumption_in_households (accessed Nov. 07, 2018).

[2] U.S. Energy Information Administration, "Table CE3.1 Annual household site end-use consumption in the U.S. — totals and averages, 2015," 2018.

[3] H. Galli, "Josef Jenni packt die Sonne in den Tank," *Der Bund*, 2013.

[4] "7.7-MWh-Speicher für weiteres Solar-MFH," 2018. https://www.gebaeudetechnik.ch/waerme-kaelte/waermetechnik/77-mwh-speicher-fuer-weiteres-solar-mfh/ (accessed Jan. 10, 2021).

[5] C. Hewicker, O. Werner, M. Ebert, T. Mennel, N. Verhaegh, and J. Raadschelders, "Energiespeicher in der Schweiz. Bedarf, Wirtschaftlichkeit und Rahmenbedingungen im Kontext der Energiestrategie 2050," 2013. Accessed: Jun. 02, 2016. [Online]. Available: http://www.news.admin.ch/NSBSubscriber/message/attachments/33125.pdf.

[6] D. Mangold and O. Miedaner, "Technisch-Wirtschaftliche Analyse Und Weiterentwicklung Der Solaren Langzeit-Wärmespeicherung." Solites, 2011.

[7] S. M. Hasnain, "Review on sustainable thermal energy storage technologies, Part I: heat storage materials and techniques," *Energy Conversion and Management*, vol. 39, no. 11, pp. 1127–1138, Aug. 1998, doi: 10.1016/S0196-8904(98)00025-9.

[8] W. Villasmil, L. J. Fischer, and J. Worlitschek, "A review and evaluation of thermal insulation materials and methods for thermal energy storage systems," *Renewable and Sustainable Energy*

Reviews, vol. 103, no. July 2018, pp. 71–84, Apr. 2019, doi: 10.1016/j.rser.2018.12.040.

[9] L. Navarro *et al.*, "Thermal energy storage in building integrated thermal systems: A review. Part 1. active storage systems," *Renewable Energy*, vol. 88, pp. 526–547, 2016, doi: 10.1016/j.renene.2015.11.040.

[10] T. Beikircher and M. Demharter, "Heat Transport in Evacuated Perlite Powders for Super-Insulated Long-Term Storages up to 300 °C," *Journal of Heat Transfer*, vol. 135, no. 5, p. 051301, 2013, doi: 10.1115/1.4023351.

[11] H. Burmeister and B. Keller, "Climate surfaces: a quantitative building-specific representation of climates," *Energy and Buildings*, vol. 28, no. 2, pp. 167–177, 1998, doi: 10.1016/S0378-7788(98)00012-7.

[12] P. Schuetz *et al.*, "Fast simulation platform for retrofitting measures in residential heating," in *Cold Climate HVAC 2018*, 2018, pp. 713–723, doi: 10.1007/978-3-030-00662-4_60.